Energy Advances

ROYAL SOCIETY OF CHEMISTRY

PAPER

View Article Online
View Journal | View Issue

Cite this: *Energy Adv.*, 2025, 4, 788

Lithiation mechanism of sulfur surfaces during discharge of Li–S batteries from quantum chemical calculations†

Jonas Lührs, Daniel Sebastiani and Pouya Partovi-Azar *

We present a computational study based on quantum-chemical calculations to investigate the initial lithiation reactions on the (001) surface of α-sulfur. The study aims to explore the possible emerging structures during consecutive lithiation steps and to analyze their reaction enthalpies. Our results show that during the first lithiation reactions, S_8 rings in the lower layers of the (001) surface are preferentially lithiated. In subsequent lithiation steps, we find that S_8 rings on the upper layers, adjacent to previously lithiated molecules, may also undergo lithiation. Once Li_2S_8 dimers are formed, further reactions on the surface can proceed, leading to the formation of Li_2S_8 trimers in a lower/upper/lower layer arrangement or lower-order Li-polysulfides, such as Li_2S_6/Li_2S_2 and Li_2S_5/Li_2S_3. Notably, in contrast to sulfur reduction reactions in the electrolyte, the formation of Li_2S_4/Li_2S_4 does not occur on the (001) surface, likely due to the surface morphology, which prevents complete exposure of S_8 rings to lithium ions. This suggests that surface lithiation predominantly leads to the formation of high-order polysulfides in the early stages of discharge, while the dissolution of these higher-order polysulfides into the electrolyte may facilitate their reduction to Li_2S_4, a process observed experimentally. Our study provides an atomistic mechanism for the discharge process of Li–S batteries with a crystalline α-sulfur cathode, contributing to a deeper understanding of both solid- and liquid-phase reactions during the early discharge stages.

Received 19th February 2025,
Accepted 24th April 2025

DOI: 10.1039/d5ya00050e

rsc.li/energy-advances

1. Introduction

The ever-increasing global energy demand calls for more efficient energy-storage devices. Currently, lithium-ion batteries are the most commonly used in electronic devices such as mobile phones, tablets, and electric cars *etc.*[1] However, the energy density of these batteries has only incrementally increased in the past decade approaching a saturated energy density of 250–400 W h kg^{-1}.[2,3] This has been made possible only by using rare metals, which increases the net weight of Li-ion batteries as well as their cost. As an alternative, lithium–sulfur (Li–S) batteries have the potential to replace Li-ion batteries due to their very high energy density of around 2600 W h kg^{-1}.[4,5] Moreover, sulfur is an abundant material, and therefore considerably cheaper[6] compared to the transition metals required for Li-ion batteries. Nevertheless, Li–S batteries still face technical issues that prevent their everyday use. These issues are partially related to the formation of soluble lithium polysulfides which result in shuttle effect during the discharge process, which is believed to be the main reason for the poor cycle life of Li–S batteries.[1,7–12]

Among the proposed cathode materials to mitigate the shuttle effect, sulfur/carbon copolymers[13–23] and covalent organic frameworks[24–30] have recently attracted much attention. Despite the promising performance of these materials to immobilize the lithium polysulfides (or even to facilitate sulfur reduction reactions), the overall electrochemical performance of the whole cathode, is determined to a great extent by that of the crystalline sulfur to which the copolymers or covalent organic frameworks are added. Therefore, to prevent the shuttle effect, it is important to gather an atomistic insight into the lithiation mechanism of crystalline sulfur. Although the main reactions during discharge are believed to occur in the solvent,[10–12,31,32] the initial lithiation reactions occur primarily on the cathode surface, as octa-sulfur is nonpolar. Additionally, previous quantum-chemical studies have addressed lithiation reaction at sulfur/solvent interface including explicit solvent molecules using *ab initio* molecular dynamics (AIMD) which suggest the occurrence of consecutive lithiation reactions at the sulfur surfaces forming lower-order Li-polysulfides, before their dissolution into the electrolyte.[33] Therefore, it is important to understand the morphological changes of the sulfur surfaces during early stages of discharge.

Van-Danckelmann-Platz 4, Halle (Saale), Germany.
E-mail: pouya.partovi-azar@chemie.uni-halle.de

† Electronic supplementary information (ESI) available. See DOI: https://doi.org/10.1039/d5ya00050e

The purpose of this study is to investigate the lithiation mechanism of the (001) surface of the crystalline α-sulfur, determine the most stable products formed during this process, and study the structural changes of the surface during lithiation using quantum chemical calculations. Despite several studies to elucidate the lithiation mechanism of solvated S_8 and on sulfur surfaces,[33–35] an atomistic understanding of the underlying processes and structural changes remains incomplete due to the complex nature of the reactions.

2. Computational details

To represent the sulfur surface, certain steps were taken to create a suitable system for geometry optimizations using density functional theory (DFT) calculations.[36] The calculations were performed on the orthorhombic α-sulfur, considering its (001) surface which, along with the (100) surface, has the lowest energy compared to other α-sulfur surfaces.[33] The original unit cell structure was extracted from X-ray diffraction measurements.[37] We employed periodic boundary conditions (PBC) along the *x* and *y* axes to represent crystallinity. In addition, a vacuum buffer along the *z*-axis was implemented to expose the (001) surface for lithiation reactions. To prevent the formation of radical electron structures, a modification was made to the top layer in the *z*-direction to ensure the absence of broken S_8 rings. Detailed information can be found in Fig. 1 and Table 1. To study lithiation reactions, we used CP2K/QUICKSTEP package,[38] incorporating dual plane-wave and Gaussian basis functions. A double-zeta plus polarization basis set optimized for molecular systems (DZVP-MOLOPT-SR-GTH)[39] was used for the valence electrons together with Goedecket–Teter–Hutter-type pseudopotentials,[40,41] and the Perdew–Burke–Ernzerhof (PBE) exchange–correlation functional.[42] To account for dispersion interactions, the DFT-D3[43] method was incorporated. Electronic structure calculations employed an SCF convergence criterion set at 10^{-6} and the atomic coordinate optimizations were conducted using the BFGS optimizer.[44–47] Our calculations including an implicit solvent model, did not show significant structural differences in the product structures of lithiation reactions in electrolyte (see ESI†). Besides, the main concern here is to understand the deformation of the sulfur surface during lithiation reactions rather than the solubility or dissociation of the lithiated products. Therefore, here we did not include an implicit solvent model for the electrolyte.

Table 1 Details on the structure of the model (001) α-sulfur surface in this study

Number of atoms	578
Unit cell size [Å]	(*a*, *b*, *c*) = (31.39, 25.73, 60.00)
Angles [°]	(α, β, γ) = (90, 90, 90)

The sulfur surface structure was prepared for the lithiation reaction by initially relaxing the sulfur slab in a vacuum. This involved relaxing the upper three layers while keeping the lower three layers fixed, as shown in Fig. 2. The relaxation of the upper layers represents the surface flexibility, which is important for the lithiation process. Meanwhile, the constraint of the lower layers mimics the crystallinity of the sulfur system. Fig. 2(a) shows the *z*-displacement of each layer during the relaxation process while (b) highlights the corresponding layers, encircled using the same color coding. The obtained relaxed structure is the starting point for the lithiation process. To study the product structures in each lithiation reaction, distinct positions for two lithium atoms were chosen on the sulfur surface. Always two lithium atoms with a distance of around 3 Å were added to different positions on the surface at

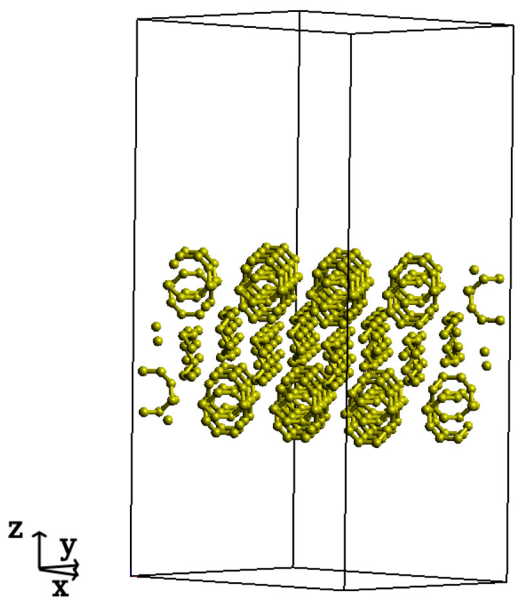

Fig. 1 Unit cell with S_8 slab. Perpendicular to the *z* axis are (001) surfaces, while PBC as used along *x* and *y* axes.

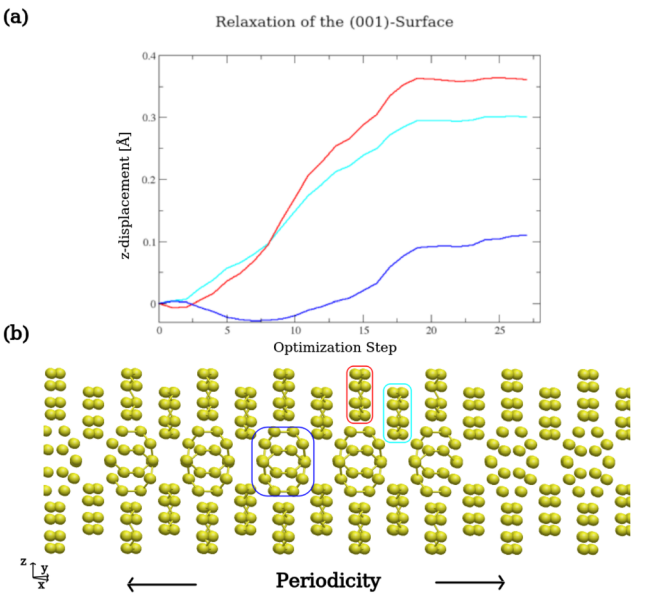

Fig. 2 (a) *z*-Displacement of the upper layers, (b) the final structure and the marked upper layers.

each lithiation step to ensure that no radical systems are present in the process of the lithiation. For each position two lithium atoms were arranged once parallel (p) and once orthogonal (o) to the (001) surface. The product structures were then obtained by optimizing the entire system, including the two lithium atoms, while constraining the lower three ring layers. Consequently, for each subsequent lithiation step, the lowest-energy product from the previous step was used as the starting point to define new distinct positions for additional lithium atoms.

The reaction energy for each lithiation step was calculated *via*

$$\Delta E_R = \frac{E_{\text{Product}} - (E_{\text{Educt}} + E_{2\text{Li}})}{2}, \quad (1)$$

where ΔE_R is the reaction energy per lithium atom. Here, neglecting entropic effects, we approximate the free energies with DFT total energies. As such, E_{Product}, E_{Educt}, and $E_{2\text{Li}}$ are the DFT energies of the optimized product structures, educt structures, and twice the energy of an isolated lithium atom, respectively. For example, in the first lithiation reaction,

$$S_8 + 2Li^+ + 2e^- \rightarrow Li_2S_8, \quad (2)$$

the product energy, E_{Product}, refers to the total energy of the system with one Li_2S_8 formed on the surface, and the educt energy, E_{Educt}, refers to the total energy of an α-sulfur slab in Fig. 1.

3. Results and discussion

In particular, we try to provide answers to the following questions:

1. How does the surface topography affect the lithiation reactions?

2. How comparable are the product structures to the known gas/liquid-phase products at each lithiation step?

3. Is the lithiation of the surface a homogeneous process or happens through nucleation?

To provide answers to these questions, we focus on the first few lithiation reactions corresponding to the early stages of discharge.

3.1. First lithiation

The periodicity of the (001) surface along x and y axes reveals two distinct S_8 rings on the surface [Fig. 3(a)]. Notably, in Fig. 3(b), one S_8 ring resides in the upper layer, while the other is positioned in the lower layer. These layers alternate on the surface and are highlighted in Fig. 3(a) and (b) as "up" and "down". The repeating unit of two S_8 rings [Fig. 3(a)] results in the recurrence of distinct positions for the lithiation reactions [Fig. 3(c)]. These distinct positions serve as representative sites for two Li atoms in the reactant structures and are expected to break one S–S covalent bond in the S_8 rings after the reaction. As such, S(1)/S(2) in Fig. 3(c) denote the upper S_8 ring, while S(3)/S(4) represent the distinct positions on the lower S_8 ring.

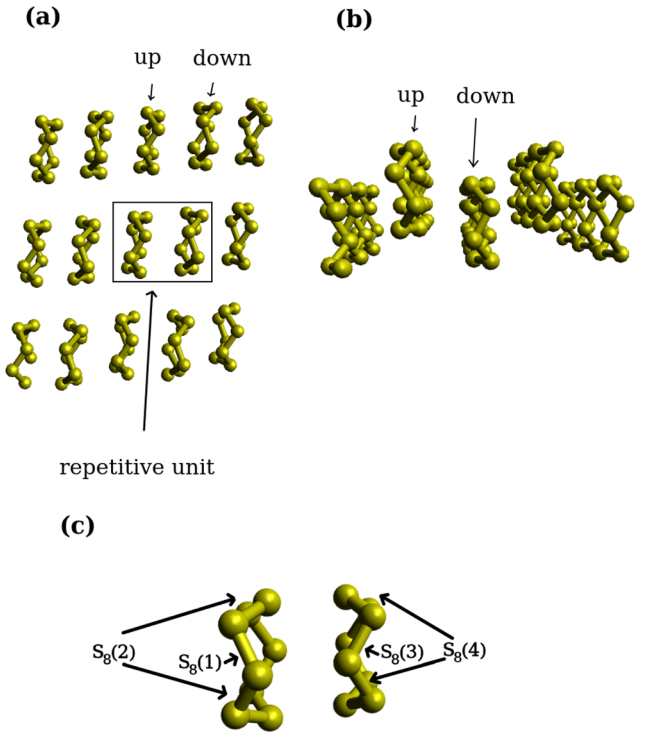

Fig. 3 First lithiation step: (a) repetitive unit of the S_8 surface from top view, (b) upper and lower layers of the S_8 surface from side view, (c) distinct positions as reaction centers.

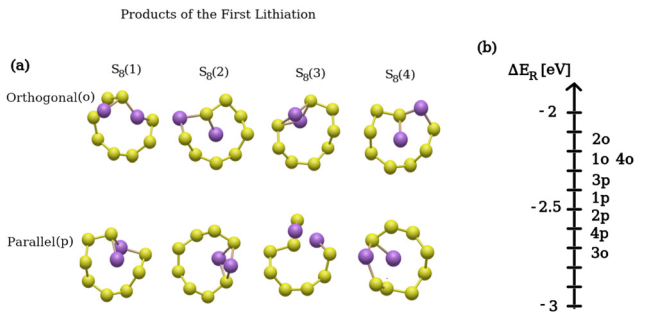

Fig. 4 First lithiation step: (a) calculated product structures after the first lithiation (only the affected S_8 ring is shown). (b) Distribution of the reaction energies. In (b), for example 4p refers to the S_8(4) structure in (a) where the two Li atoms were initially positioned in parallel with respect to the (001) surface.

Fig. 4(a) presents the product structures of the first lithiation reaction (only the affected S_8 ring is shown), while Fig. 4(b) shows the reaction energy distribution of all the possible products. In Fig. 4(b), for example, 4p refers to the S_8(4) structure in (a) where the two Li atoms were initially placed in a parallel configuration with respect to the (001) surface. The difference in reaction energies between the product structures is significant, namely up to 0.7 eV per lithium atom. This is due to the fact that the molecular structure of each product is sizably different. The energy distributions of the subsequent lithiation steps (*i.e.* second and third) were not shown as the reaction energy ranges were found to be similar to the energy

Table 2 Sulfur–lithium distances [Å] of Li_2S_8 computed on the (001) α-sulfur surface and in the gas phase[48]

Structure	S(1)–Li(1)	S(2)–Li(1)	S(1)–Li(2)	S(2)–Li(2)
2p	2.35	2.38	2.45	2.38
3o	2.40	2.41	2.38	2.41
Ref. 48	2.44	2.44	2.44	2.44

distribution in Fig. 4(b). Despite their similar configuration (Table 2), the 2p product structure on the upper ring corresponds to a lithiation reaction with a reaction energy ∼0.21 eV higher than that of the 3o product structure on the lower ring. Based on these results, it can be concluded that lower S_8 rings are energetically preferred for lithiation compared to upper ones. This conclusion was additionally validated for the following lithiation steps with a broader sample size of initial geometries.

Another important point to note is that the optimal structures closely resembled the Li_2S_8 structure in the gas/liquid phase, as shown in Table 2. The previous gas/liquid-phase results,[48] were obtained on a ring-shaped structure where a mesomeric rhombus forms *via* two similar Li–S bonds after the lithiation. These observations also align with the 2p and 3o structures obtained here. Additionally, we calculated the product structures corresponding to the gas- and liquid-phase lithiation reactions and are reported in the ESI.† Our results also showed a diamond-shaped structure for Li_2S_8 with slightly different bond angles and distances compared to those reported in ref. 48. Besides, the structural differences between gas- and liquid-phase structures are marginal (see Fig. S5 and Table S2 in the ESI†). On the (001) surface, the Li_2S_8 structures of 2p and 3o also exhibit equidistant Li–S bonds and form a mesomeric rhombus structure. They also result in a ring-shaped product structure. Here, the 3o structure, corresponding to a lithiation reaction with the lowest reaction energy, was considered as the initial structure for the next lithiation step.

3.2. Second lithiation

For the second reaction, two possibilities can be considered: (i) a neighboring ring undergoes a lithiation; or (ii) the Li_2S_8 becomes further lithiated to two lower-order polysulfides. These correspond to the following two reactions,

$$S_8 + 2Li^+ + 2e^- \rightarrow Li_2S_8$$

$$Li_2S_8 + 2Li^+ + 2e^- \rightarrow Li_2S_{8-x}/Li_2S_x, \quad (3)$$

where x in the equation can have any value between 1 and 7 as these are the known conformations of Li-polysulfides,[48] and "/" represents a cluster-type structures, meaning they can not be seen as two isolated structures.

For the second lithiation, two different classes of distinct positions were selected. Firstly, positions surrounding the previously lithiated Li_2S_8 ring, and secondly, positions around intact S_8 rings. The positions surrounding the Li_2S_8 molecule were selected in such a way that the new Li atoms are allowed to attack S–S bonds of the Li_2S_8 molecule which are accessible on the surface. Due to its asymmetrical geometry, the accessible

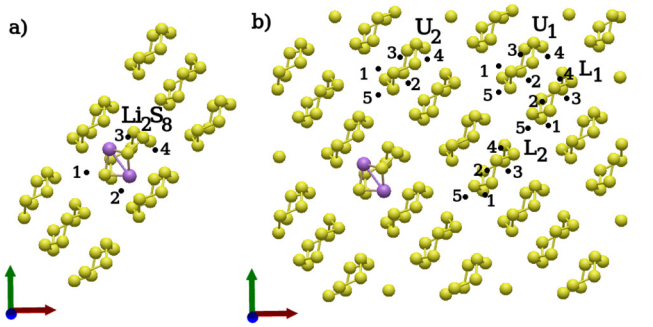

Fig. 5 Second lithiation step: distinct positions considered for the second lithiation. (a) Distinct positions around an Li_2S_8 molecule. (b) Distinct positions around an intact S_8.

bonds on both sides of every Li_2S_8 molecule were considered. For the intact S_8 molecules, positions were chosen to ensure that the rings are not adjacent to the lithiated ones. The chosen positions are identical to those used in the previous lithiation step, with the exception that an additional position was considered closest to the already lithiated center. Moreover, positions on both sides of each S–S bond were considered to account for all lithiation possibilities. Two S_8 molecules in the lower layer (L) and two S_8 rings in the upper layer (U) were chosen [Fig. 5(b)]. It is worth mentioning that, in the second lithiation, the use of 'U' for upper and 'L' for lower sulfur layers in Fig. 5 refers only to the initial structures. This implies that the position of the two Li atoms on an upper layer could result in a polysulfide product structure formed on the lower layer and *vice versa*. Although such an occurrence was observed to happen rarely, it was taken into account for the average energy calculation of upper- and lower-layer conformations, as well as for comparing structures.

Fig. 6 shows the lowest-reaction energy structures formed on the upper and lower sulfur layers. We observe that the two Li atoms around the Li_2S_8 ring do react with the upper neighboring rings but not with the already lithiated one. While the direct subsequent lithiation of the already lithiated ring is in principle possible, it appears to be less likely. The underlying reason could be that the lithiated ring is strongly protected by the surrounding pristine S_8 rings of the surface, and the only exposed site is where the two lithium atoms from the first lithiation step are located. Hence, the reactivity of the Li_2S_8 ring in a second lithiation step is low, and the second lithiation step is more likely to occur at neighboring S_8 rings. Li_2S_8 1p describes the product of sulfur ring in an upper layer [Fig. 6] interacting with the adjacent Li_2S_8 ring from the lower layer. Therefore, Li_2S_8 emerges as the only stable product of the second lithiation step, as the lithiation around an Li_2S_8 molecule from the first lithiation step leads to the formation of a Li_2S_8 dimer. As such, only the first reaction in (3) seems to be thermodynamically likely.

Table 3 represents Li–S distances in these product structures, namely L_1 1p, L_2 3o, and Li_2S_8 1p, for comparison with a Li_2S_8 molecule in the gas phase. All products have comparable Li–S bond distances, with an average bond length of ∼2.40 Å.

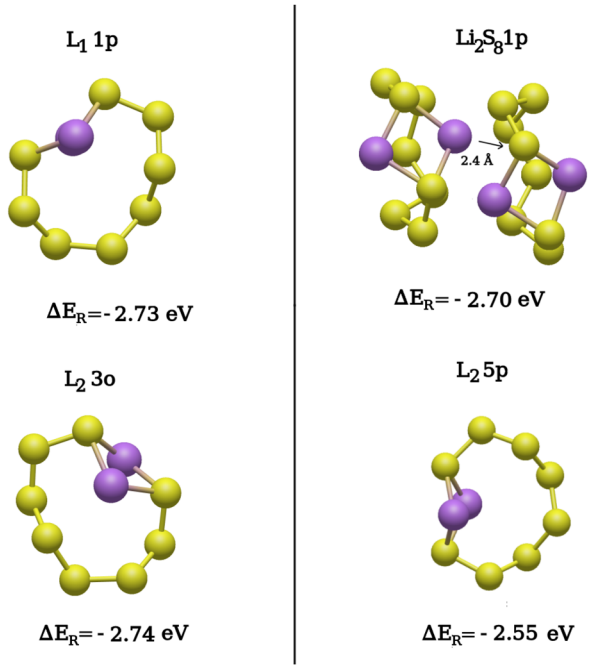

Fig. 6 Second lithiation step: comparison of the lowest-reaction energy structures formed on the lower (left) and the upper (right) sulfur layers. Li_2S_8 1p refers to the product of the lithiation reaction on an adjacent sulfur ring to the already lithiated one. The others are isolated rings.

Table 3 Lithium–sulfur distances [Å] of Li_2S_8 formed on the (001) α-sulfur surface in the second lithiation step, and comparison with those in the gas/liquid phase

Structure	S(1)–Li(1)	S(2)–Li(1)	S(1)–Li(2)	S(2)–Li(2)
Li_2S_8 1p	2.43	2.42	2.37	2.35
L_2 3o	2.42	2.39	2.38	2.43
L_1 1p	2.39	2.42	2.38	2.38
Ref. 48	2.44	2.44	2.44	2.44

Their atomic configurations are also similar to an Li_2S_8 molecule in the gas phase. The reaction energies of all structures are also similar, with the product structures L_2 3o and L_1 1p being around 50 meV lower in energy than Li_2S_8 1p obtained through lithiation around Li_2S_8. A closer look reveals that structures L_2 3o and L_1 1p (two Li_2S_8 rings far away from each other) are the products of lithiation of two distant S_8 rings both in lower layers. We also observe that the L_2 5p product structure consisting of two Li_2S_8 rings both on lower layers shows about 200 meV higher reaction energy than L_2 3o, L_1 1p, and Li_2S_8 1p. One possible reason for this is that in the Li_2S_8 1p product structure, the lithium atoms can interact strongly with the lone-pair electrons on the terminal sulfur atoms from the neighboring Li_2S_8 ring [Fig. 6, top-right panel].

Compared to the first lithiation, the reaction energies of L_1 1p and L_2 3o are similar to that of the product of the first lithiation. This is expected since they occur on isolated S_8 rings. For the next lithiation step, the product structure Li_2S_8 1p was selected, because even though the other two structures (L_1 1p and L_2 3o) correspond to a slightly lower reaction energies, they would only represent a similar starting structure as for the second lithiation.

3.3. Third lithiation

Here, all possible reaction paths for a third lithiation step are considered as following

$$S_8 + 2Li^+ + 2e^- \rightarrow Li_2S_8$$

$$Li_2S_8 + 2Li^+ + 2e^- \rightarrow Li_2S_7/Li_2S$$

$$Li_2S_8 + 2Li^+ + 2e^- \rightarrow Li_2S_6/Li_2S_2$$

$$Li_2S_8 + 2Li^+ + 2e^- \rightarrow Li_2S_5/Li_2S_3$$

$$Li_2S_8 + 2Li^+ + 2e^- \rightarrow Li_2S_4/Li_2S_4 \quad (4)$$

As before, several S_8 rings and prelithiated Li_2S_8 structures were considered as potential reaction sites. The positions for the two additional Li atoms around the preexisting Li_2S_8 are shown in Fig. 7(a). The structures of the two neighboring Li_2S_8 rings are sizably different from a single Li_2S_8 molecule in the gas phase. Therefore, different positions for the two Li atoms are evenly distributed around the Li_2S_8 rings. Here, the positions 1–4, 11–12 are around the upper Li_2S_8 ring and 5–9 around the lower one [Fig. 7(a)]. For the distinct positions around an intact S_8 in Fig. 7(b), lower layer rings (L_1, L_4) adjacent to the two Li_2S_8 molecules and those farther away (L_2, L_3) from them are considered. The same procedure was applied for the upper S_8 rings in Fig. 7(c). The lithiation process on isolated rings (L_2, L_3 and U_2, U_3) only result in Li_2S_8 molecules similar to the previous lithiation steps. However, a third lithiation reaction adjacent and on the two Li_2S_8 rings (L_1, L_4 and U_1, U_4, Li_2S_8) results in more complex structures, such as Li_2S_7/Li_2S, Li_2S_6/Li_2S_2 and Li_2S_5/Li_2S_3 clusters and bridged structures like Li_2S_8/Li_2S_8. Atomic coordinate optimizations of the reactant structures mostly result in Li_2S_7/Li_2S and Li_2S_6/Li_2S_2 complexes while clusters of Li_2S_4/Li_2S_4 are not observed. One explanation for the absence of Li_2S_4/Li_2S_4 clusters

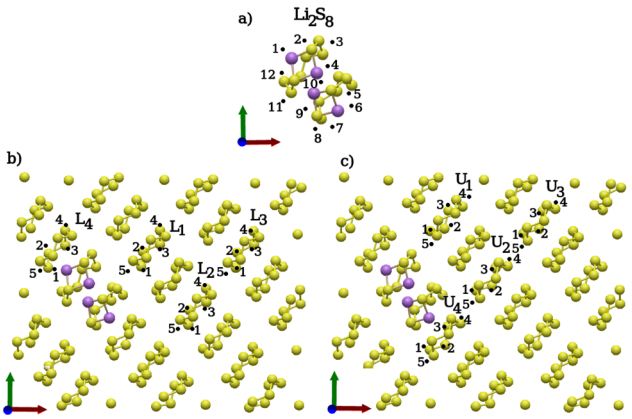

Fig. 7 Third lithiation step: distinct positions on the (001) α-sulfur surface considered for the third lithiation reaction, (a) around Li_2S_8 dimer obtained in the previous lithiation step, (b) on the lower layers, and (c) on the upper layers around the dimer.

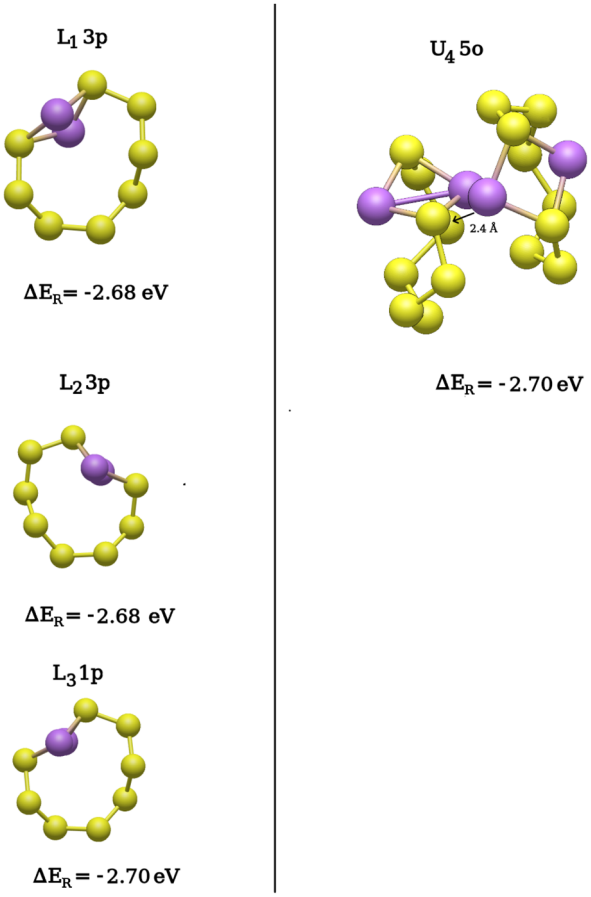

Fig. 8 Third lithiation step: comparison of the structures with the lowest reaction energies formed on the lower (left) and the upper (right) layers of the (001) surface.

is that the S–S bonds are not accessible to the two Li atoms due to their location beneath the reachable surface. This is in stark contrast to the gas/liquid-phase reactions. Without exception, the structures of the isolated or non-interacting Li_2S_8 molecules with the lowest reaction energies are those that are most similar to Li_2S_8 in the gas phase [Fig. 8]. This is consistent with the first and second lithiation steps.

We observe that in cases where an adjacent S_8 ring is lithiated, the atomic configuration of the emerging Li_2S_8 cluster is very different from the monomers in the gas phase. Therefore, the comparison of the lowest-reaction energy structures to the Li_2S_8 molecules in the gas phase is only possible when the Li_2S_8 molecule is not directly interacting with other Li-polysulfides. This is illustrated in Fig. 9, where a distorted structure called Li_2S_8 7p is shown corresponding to a lower reaction energy than a similar gas-phase structure. The formation of Li_2S_8 7p might be an indicator that it is thermodynamically preferred that the lithiated structure forms on a lower adjacent S_8 ring where the two Li atoms are exposed to the terminal S atoms of the neighboring Li_2S_8 ring [Fig. 9].

Quite comparable in reaction energies to the product structures such as Li_2S_8 7p and L_4 3p [Fig. 9] are the cluster/bridged structures shown in Fig. 10.

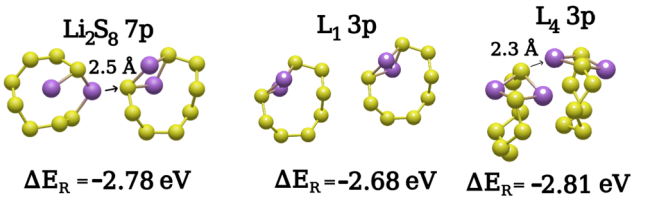

Fig. 9 Third lithiation step: comparison of two Li_2S_8 adjacent structures formed during the third lithiation reaction.

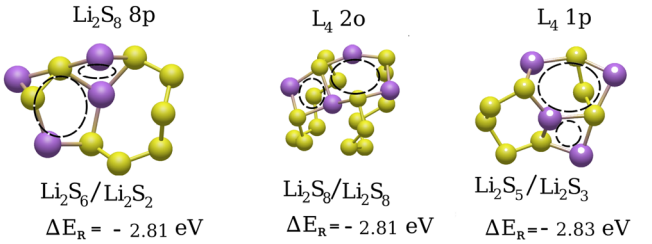

Fig. 10 Third lithiation step: mesomeric structures.

Of all the cluster and bridged structures, only those with the lowest reaction energies are presented in Fig. 10. For example, the Li_2S_7/Li_2S family of product structures [see reactions (4)], which exhibit considerably higher reaction energies, are not shown. All of these structures display a specific mesomeric pattern, as indicated by the dashed lines in Fig. 10. The results highlight two distinct types of lithiation products: those involving two lithiated Li_2S_8 rings (L_4 2o) and those where an already lithiated Li_2S_8 molecule undergoes further lithiation (Li_2S_8 8p and L_4 1p). Additionally, some cluster structures, such as Li_2S_6/Li_2S_2 (Fig. S1 in the ESI†), exhibit similar mesomerism but have higher reaction energies, likely due to strong electrostatic repulsion between closely positioned lithium atoms.

Despite these observations, the third lithiation step exhibits limited predictive insights onto the preferred conversion pathway due to comparable reaction energies across multiple product configurations. While mesomeric structures and lower adjacent Li_2S_8 products are thermodynamically favored, Li_2S_7/Li_2S formation is energetically unfavorable on the sulfur surface. Additionally, Li_2S_4 dimerization is precluded by steric hindrance, as simultaneous Li^+ diffusion beneath Li_2S_8 structures to access buried S–S bonds is geometrically restricted. Reactivity trends further indicate that lower adjacent S_8 rings exhibit a higher lithiation propensity compared to isolated or upper-layer rings. This is likely due to reduced Li^+ migration barriers and cooperative interactions with neighboring intermediates. While definitive reaction pathways remain unresolved, these insights help narrow plausible mechanisms by eliminating improbable reactions (*e.g.*, Li_2S_7 formation) and identifying preferred structural motifs (*e.g.*, adjacent Li_2S_8 interactions). Ultimately, our findings suggest that lower-lying Li_2S_8 rings interacting with already lithiated S_8 molecules, as well as Li-polysulfide cluster-type structures such as Li_2S_6/Li_2S_2 or Li_2S_5/Li_2S_3, are the most favorable products of the third lithiation step.

4. Conclusions

Our study provides a detailed atomistic insight into the initial lithiation process on the (001) surface of -sulfur, offering a fundamental understanding of the early-stage reactions in Li–S batteries. The findings suggest that lithiation preferentially begins with S_8 rings on the lower layer of the surface, leading to the formation of Li_2S_8 molecules. These surface-stabilized Li_2S_8 molecules exhibit strong similarities to their counterparts in gas/liquid-phase lithiation, indicating that early surface lithiation plays a critical role in determining subsequent reaction pathways. As lithiation progresses, further reactions around Li_2S_8 dimers lead to the formation of Li-polysulfides, including Li_2S_6, Li_2S_5, and lower-order species like Li_2S_3 and Li_2S_2. Notably, the formation of Li_2S_4 is sterically hindered on the surface, which may explain its preferential formation in the liquid phase. The dissolution of higher-order polysulfides into the electrolyte could further drive their reduction, reinforcing the experimentally observed discharge mechanism. These insights contribute to a deeper understanding of solid–liquid interactions during Li–S battery discharge and highlight the significance of surface lithiation in shaping polysulfide evolution.

Therefore, the current study presents a detailed atomistic picture of the first lithiation reactions on the (001) surface of α-sulfur and suggests a discharge mechanism of Li–S batteries with crystalline sulfur cathode which can contribute to a better understanding of such a complex process involving both solid- and liquid-phase reactions.

Author contributions

J. L. contributed to formal analysis, investigation, methodology, visualization, and writing (original draft, review & editing); D. S. contributed to supervision, validation, and writing (review & editing); P. P.-A. contributed to conceptualization, funding acquisition, methodology, supervision, validation, and writing (review & editing).

Data availability

All data and code supporting this study are publicly available at **https://github.com/jolu75/Data**. The data were curated and maintained by J. Lührs.

Conflicts of interest

There are no conflicts to declare.

Acknowledgements

This work was primarily supported by the Deutsche Forschungsgemeinschaft (DFG, German Research Foundation) through the RTG BEAM (project number 329482734). The authors gratefully acknowledge DFG funding *via* projects PA3141/3 (project number 420536636), PA3141/5 (project number 446879138). The authors also acknowledge the computing time made available on the high-performance computer at the NHR Center of TU Dresden *via* the project 'p_oligothiophenes'. This center is jointly supported by the Federal Ministry of Education and Research and the state governments participating in the NHR (**https://www.nhr-verein.de/unsere-partner**). P. P.-A. also gratefully acknowledges Rafael Müller for fruitful discussions.

Notes and references

1 M. Wild and G. Offer, *Lithium–Sulfur Batteries*, Wiley, London UK, 1st edn, 2019.
2 P. Stenzel, M. Baumann, J. Fleer, B. Zimmermann and M. Weil, 2014 IEEE International Energy Conference (ENERGYCON), 2014.
3 G. E. Blomgren, *J. Electrochem. Soc.*, 2016, **164**, A5019–A5025.
4 K. Amine, R. Kanno and Y. Tzeng, *MRS Bull.*, 2014, **39**, 395–401.
5 Y. Jin, K. Liu, J. Lang, X. Jiang, Z. Zheng, Q. Su, Z. Huang, Y. Long, C.-A. Wang, H. Wu and Y. Cui, *Joule*, 2020, **4**, 262–274.
6 A. Rosenman, E. Markevich, G. Salitra, D. Aurbach, A. Garsuch and F. F. Chesneau, *Adv. Energy Mater.*, 2015, **5**, 1500212.
7 Y. V. Mikhaylik and J. R. Akridge, *J. Electrochem. Soc.*, 2004, **151**, A1969.
8 Y. Huang, L. Lin, C. Zhang, L. Liu, Y. Li, Z. Qiao, J. Lin, Q. Wei, L. Wang, Q. Xie and D. Peng, *Adv. Sci.*, 2022, **9**, 2106004.
9 R. Xu, I. Belharouak, X. Zhang, R. Chamoun, C. Yu, Y. Ren, A. Nie, R. Shahbazian-Yassar, J. Lu, J. C. Li and K. Amine, *ACS Appl. Mater. Interfaces*, 2014, **6**, 21938–21945.
10 T. D. Pham, *et al.*, *Small*, 2024, **20**, 202307951.
11 Y. Lin, J. Zheng, C. Wang and Y. Qi, *Nano Energy*, 2020, **75**, 104915.
12 J. L. D. Salvo, G. L. Luque and G. D. Luca, *Mol. Syst. Des. Eng.*, 2022, **7**, 364–373.
13 P. Partovi-Azar, S. Panahian Jand and P. Kaghazchi, *Phys. Rev. Appl.*, 2018, **9**, 014012.
14 J. Shen, Y. Feng, P. Wang, G. Qiu, L. Zhang, L. Lu, H. Wang, R. Wang, V. Linkov and S. Ji, *ACS Sustainable Chem. Eng.*, 2020, **8**, 10389–10401.
15 C.-J. Huang, J.-H. Cheng, W.-N. Su, P. Partovi-Azar, L.-Y. Kuo, M.-C. Tsai, M.-H. Lin, S. P. Jand, T.-S. Chan and N.-L. Wu, *et al.*, *J. Power Sources*, 2021, **492**, 229508.
16 Q. Zhang, Q. Huang, S.-M. Hao, S. Deng, Q. He, Z. Lin and Y. Yang, *Adv. Sci.*, 2022, **9**, 2103798.
17 P. Partovi-Azar, *Phys. Rev. Appl.*, 2022, **18**, 044072.
18 R. Kiani, D. Sebastiani and P. Partovi-Azar, *ChemPhysChem*, 2022, **23**, e202100519.
19 S. de Kock, K. Skudler, R. Matsidik, M. Sommer, M. Müller and M. Walter, *Phys. Chem. Chem. Phys.*, 2023, **25**, 20395–20404.
20 H. Raza, S. Bai, J. Cheng, S. Majumder, H. Zhu, Q. Liu, G. Zheng, X. Li and G. Chen, *Electrochem. Energy Rev.*, 2023, **6**, 29.

21 R. Kiani, M. Steimecke, M. Alqaisi, M. Bron, D. Sebastiani and P. Partovi-Azar, *RSC Adv.*, 2023, **13**, 27756–27763.
22 Y. Schütze, D. Gayen, K. Palczynski, R. de Oliveira Silva, Y. Lu, M. Tovar, P. Partovi-Azar, A. Bande and J. Dzubiella, *ACS Nano*, 2023, **17**, 7889–7900.
23 R. Kiani, H. Sheng, T. Held, O. Löhmann, S. Risse, D. Sebastiani and P. Partovi-Azar, *ChemPhysChem*, 2024, e202400681.
24 H. Liao, H. Ding, B. Li, X. Ai and C. Wang, *J. Mater. Chem. A*, 2014, **2**, 8854–8858.
25 Z.-J. Zheng, H. Ye and Z.-P. Guo, *Energy Environ. Sci.*, 2021, **14**, 1835–1853.
26 Z. Wang, F. Pan, Q. Zhao, M. Lv and B. Zhang, *Front. Chem.*, 2022, **10**, 1055649.
27 R. Yan, B. Mishra, M. Traxler, J. Roeser, N. Chaoui, B. Kumbhakar, J. Schmidt, S. Li, A. Thomas and P. Pachfule, *Angew. Chem., Int. Ed.*, 2023, **62**, e202302276.
28 B. Hu, J. Xu, Z. Fan, C. Xu, S. Han, J. Zhang, L. Ma, B. Ding, Z. Zhuang and Q. Kang, *et al.*, *Adv. Energy Mater.*, 2023, **13**, 2203540.
29 S. Lv, X. Ma, S. Ke, Y. Wang, T. Ma, S. Yuan, Z. Jin and J.-L. Zuo, *J. Am. Chem. Soc.*, 2024, **146**, 9385–9394.
30 Z. Wang, X. Wu, S. Wei, Y. Xie and C.-Z. Lu, *Chem. Mater.*, 2024, **36**, 2412–2419.
31 P. P. R. M. L. Harks, C. B. Robledo, T. W. Verhallen, P. H. L. Notten and F. M. Mulder, *Adv. Energy Mater.*, 2016, **7**, 1601635.
32 T. Ma, *et al.*, *Angew. Chem., Int. Ed.*, 2023, **62**, e202310761.
33 C. Arneson, Z. D. Wawrzyniakowski, J. T. Postlewaite and Y. Ma, *J. Phys. Chem. C*, 2018, **122**, 8769–8779.
34 L. Wang, T. Zhang, S. Yang, F. Cheng, J. Liang and J. Chen, *J. Energy Chem.*, 2013, **22**, 72–77.
35 R. Xu, J. Lu and K. Amine, *Adv. Energy Mater.*, 2015, **5**, 1500408.
36 W. Kohn and L. J. Sham, *Phys. Rev.*, 1965, **140**, A1133–A1138.
37 S. C. Abrahams, *Acta Crystallogr.*, 1955, **8**, 661–671.
38 J. VandeVondele, M. Krack, F. Mohamed, M. Parrinello, T. Chassaing and J. Hutter, *Comput. Phys. Commun.*, 2005, **167**, 103–128.
39 J. VandeVondele and J. Hutter, *J. Phys. Chem.*, 2007, **127**, 114105.
40 S. Goedecker, M. Teter and J. Hutter, *Phys. Rev. B: Condens. Matter Mater. Phys.*, 1996, **54**, 1703–1710.
41 M. Krack, *Theor. Chem. Acc.*, 2005, **114**, 145–152.
42 J. P. Perdew, K. Burke and M. Ernzerhof, *Phys. Rev. Lett.*, 1996, **77**, 3865–3868.
43 S. Grimme, J. Antony, S. Ehrlich and H. Krieg, *J. Phys. Chem.*, 2010, **132**, 154104.
44 C. G. Broyden, *IMA J. Appl. Math.*, 1970, **6**, 76–90.
45 R. Fletcher, *Comput. J.*, 1970, **13**, 317–322.
46 D. Goldfarb, *Math. Comput.*, 1970, **24**, 23–26.
47 D. F. Shanno, *Math. Comput.*, 1970, **24**, 647–656.
48 M. Cheviri and S. Lakshmipathi, *Comput. Theor. Chem.*, 2021, **1202**, 113323.